Transport Properties of Wormlike Chains with Applications to Double Helical DNA and Carbon Nanotubes

Marc L. Mansfield*,† and Jack F. Douglas*,‡

Department of Chemistry and Chemical Biology, Stevens Institute of Technology, Hoboken, New Jersey 07030, and Polymers Division, National Institute of Standards and Technology, Gaithersburg, Maryland 20899

Received December 20, 2007; Revised Manuscript Received April 25, 2008

ABSTRACT: Many extended threadlike polymeric structures (e.g., certain synthetic polymers, carbon nanotubes, double helical DNA, and certain polypeptides) exhibit a degree of chain-stiffness intermediate between the idealized rod and the random coil. Such structures can be reasonably well described by the wormlike chain model, and we apply our previously developed numerical path-integration method to determine both the intrinsic viscosity $[\eta]$ and the friction coefficient f of wormlike chains. We have also determined finite-thickness contributions to the volume and the radius of gyration and developed approximants for $[\eta]$ and f that should be useful in characterization work. Our results are compared to previous computations of $[\eta]$ and f and the uncertainties of the various computational methods for calculating these transport properties are considered. Our results are also compared to experimental viscometric, sedimentation, and light scattering results for double helical DNA, where we obtain accurate fits by assuming a hydrodynamic diameter of $d = 2.4$ nm and a persistence length of $a = 50$ nm. Computations are also performed for a region of parameter space that should be useful in the characterization of carbon nanotubes.

1. Introduction

The wormlike chain model provides a reasonable representation of semiflexible polymers, or polymers that are insufficiently flexible to behave as random coils.[1,2] In particular, it is regarded as an excellent model of molecules such as double-helical DNA, α-helical polypeptides, nanotubes, and other stiff chains, whenever such chains are long enough that their inherent flexibility leads to departures from rigid-rod behavior but are yet too short to be represented as a random coil. Chain flexibility in the wormlike chain model is tunable between these two extreme limits.

The transport properties of polymer solutions are extremely important in polymer characterization and in the physics of polymers. These properties include the translational diffusivity, the translational friction coefficient (both of which are given in terms of the hydrodynamic radius), and the intrinsic viscosity. Kirkwood−Riseman theory[2,3] is the standard method for computing these properties, but analytical calculations are difficult and all existing treatments must introduce approximations. This is true even for the relatively simple wormlike chain model, including the classic work of Hearst and Stockmayer,[4] Ullman,[5,6] and Yamakawa and Fujii[7,8] and more recent contributions from Yamakawa's group,[9−13] which rely on a slender-body approximation for the chain backbone (see Discussion below). Recently, a new method has become available, namely a path-integration technique based on an analogy between hydrodynamics and electrostatics, which permits accurate determination of both the hydrodynamic radius and the intrinsic viscosity of macromolecules, nanoparticles, and essentially any other particle of arbitrary shape,[14−22] without having to introduce the slender-body or "string of beads" approximation just mentioned. The analogy derives from the fact that the Oseen tensor, which plays the role of a hydrodynamic Green's function, when averaged over orientations, becomes the scalar $1/(6\pi\eta r)$, which is of course proportional to the electrostatic Green's function. Replacing the latter by the former maps the hydrodynamic boundary-value problem onto an analogous electrostatic boundary-value problem, and will be referred to hereafter as the "electrostatic approximation". For example, to within the accuracy of the electrostatic approximation, the charge distribution over the surface of an arbitrarily shaped, charged conductor is proportional to the Stokes-flow force distribution over the surface of a rigid body of the same size and shape as the conductor. The capacity, C, of an arbitrary conducting body is the proportionality constant between the total charge on the body and its electrostatic potential, and has units of length. The polarizability tensor, $\boldsymbol{\alpha}$, represents the proportionality between induced dipole moment on the conducting body and applied external electric field, and has units of volume. We define $\mathrm{Tr}(\boldsymbol{\alpha})$ to be the trace of $\boldsymbol{\alpha}$, and $\langle\alpha\rangle = \mathrm{Tr}(\alpha)/3$ to be the mean polarizability. Then again, to within the accuracy of the electrostatic approximation, the capacity and mean polarizability are respectively proportional to the hydrodynamic radius and the intrinsic viscosity. The relationship between capacity and hydrodynamic radius is defined as,

$$R_h = q_h C \tag{1}$$

The relationship between polarizability and intrinsic viscosity involves an intermediate dimensionless parameter, the "intrinsic conductivity," $[\sigma] = \langle\alpha\rangle/V$ (so-called because it represents the leading virial coefficient for the electrical conductivity of a suspension of conducting particles in a medium of much lower conductivity). The relationship between $[\sigma]$ and $[\eta]$ can similarly be written as a proportionality

$$[\eta] = q_\eta[\sigma] = q_\eta \frac{\langle\alpha\rangle}{V} \tag{2a}$$

where we let $[\eta]$ represent the "volume-normalized" intrinsic viscosity. We also write

$$[\eta]_P = q_\eta \frac{V}{m}[\sigma] = q_\eta \frac{\langle\alpha\rangle}{m} = q_\eta \frac{N_A\langle\alpha\rangle}{M} \tag{2b}$$

for the "practical," or "mass-normalized" intrinsic viscosity. (The intrinsic viscosity is the leading virial coefficient of the solution

* Corresponding authors. E-mail: (M.L.M.) marc.mansfield@stevens.edu; (J.F.D.) jack.douglas@nist.edu.
† Department of Chemistry and Chemical Biology, Stevens Institute of Technology.
‡ Polymers Division, National Institute of Standards and Technology.

10.1021/ma702837v CCC: $40.75
Published on Web 06/25/2008

viscosity; $[\eta]$ emerges if we measure concentration as volume fraction and $[\eta]_P$ arises if we measure concentration as mass concentration. The first definition is dimensionless while the second has units of volume/mass and is the standard intrinsic viscosity of polymer science.) Here m, V, M, and N_A are respectively the mass, volume, molar mass, and Avogadro's number. Because the approximation is not exact, the proportionality constants q_h and q_η are weakly shape-dependent, but precise calculations[18,19] for a wide variety of shapes indicate that each lies within a narrow interval:

$$q_h = 1.00 \pm 0.01 \tag{3a}$$

$$q_\eta = 0.79 \pm 0.04 \tag{3b}$$

These front-factors are dimensionless, and since q_h is generally near unity, we treat R_h and C as interchangeable.

In addition to the relationships embodied in eqs 1 and 2, both C and α have several other physical applications. For example, C governs both the rate at which heat diffuses from a body at fixed temperature into the surrounding medium and the Smoluchowski rate constant for diffusive flux of of chemical species to or from a body. Indeed, the relationship of eq 1 between C and R_h can be viewed as arising from the diffusion of momentum away from the particle in Stokes flow. Likewise, the polarizability is related to the electrical or thermal conductivity of a suspension of good conductors suspended in a medium having a relatively poor conductivity (e.g., metal particles in polymer matrices). The relationship of eq 2 arises because the application of shear to a fluid with suspended particles of general shape creates a stress dipole ("stresslet") that reacts upon the applied field in much the same way that a conducting particle perturbs an electric field.

The evaluation of the electrostatic properties C and α is a notoriously difficult mathematical problem for particles of arbitrary shape. Therefore, the analogy would not be particularly valuable except for the fact that a path-integration technique has been developed that permits determination of C and α for arbitrary shapes.[14–22] The path-integration technique exploits an exact relation between electrostatics and the statistics of random flights, and involves the Monte Carlo sampling of random flight trajectories in the space outside the body. It determines C and α simultaneously; i.e., there is no additional overhead required to compute both over that required to calculate either one, and is exact for C and α in the infinite sampling limit. Then, we apply eq 1 to eq 3 to determine the hydrodynamic radius and the intrinsic viscosity.[23] According to eq 3, this involves about 1% and 5% uncertainty, respectively, in the hydrodynamic radius and the intrinsic viscosity. An additional source of uncertainty is finite sampling error. However, the approach is very versatile[24] and faster than standard finite-element solutions of either the equivalent electrostatic or hydrodynamic boundary-value problems, respective computation times being $O(N)$ and $O(N^3)$, for N the number of finite elements.

We note that the "electrostatic approximation" is actually relatively common in hydrodynamic calculations.[3] It is applied, for example, in deriving the well-known Kirkwood double sum formula,[2,3] as well as in earlier treatments of wormlike chains.[5–8,10–12] In other words, many workers, while trying to calculate friction or intrinsic viscosity, have actually been approximating either the capacity or the polarizability. Our approach differs from earlier applications of the electrostatic approximation in two ways: First, we determine the electrostatic properties accurately, with no additional approximations beyond sampling error, and second, because the electrostatic approximation has now been tested in numerically accurate calculations on many shapes, we are able to state its accuracy with confidence, as in eq 3. We also avoid the slender-body approximation in which the chain is represented as a string of beads, which can lead to appreciable errors in some cases.[25]

Obviously, the wormlike chain has conformational flexibility, while as mentioned above, the technique is directly applicable only to rigid particles. We use the "Zimm rigid-body approximation" to treat conformational flexibility, which asserts that the transport properties of a flexible body can be evaluated as an ensemble average over conformations, treating each conformation as a rigid body.[26] Most computations of the transport properties of polymers in solution also invoke the rigid-body approximation, and this undoubtedly introduces some uncertainty into transport property estimates.[27,28] The rigid-body approximation is probably most severe for flexible chains where the fluctuations in the friction coefficient and the intrinsic viscosity with polymer conformation are particularly large (the ensemble then comprising both compact and extended configurations). An examination of the transport properties of such chains in our previous papers[21,25] indicates that our estimates are consistent with those of Zimm,[26] who treats flexible chains as strings of hydrodynamic beads without invoking configurational or orientational preaveraging. Moreover, both our computations[21,25] and the bead model calculations[26] of flexible polymers seem to agree well with experimental observations on real flexible polymers. Taken together, these results strongly suggest that the rigid body approximation is reasonable for flexible polymers. For semiflexible or rigid-rod polymer structures, such as those which are the focus of the present paper, the fluctuations in transport properties that accompany conformational fluctuations are much smaller and we can then expect the rigid-body approximation to be an excellent approximation. Our calculations below for DNA confirm this expectation. Tanaka, et al.[13] have also tested it for bent rods. We also note that this approximation will apply well to the important case of carbon nanotubes, which are relatively rigid in comparison to most other polymeric structures. However, as we explain elsewhere,[29] some care must be exercised in performing ensemble averages of the polarizability. In the future, it should be possible to explore the influence of chain flexibility in polymer structures by molecular or Brownian dynamics, and we look forward to comparing such results with predictions of the rigid-body approximation once reliable computations become available.

As already mentioned, native double helical DNA is widely believed to be well represented by the wormlike chain model. We show below that our results are in good agreement with the sedimentation, viscosity, and light scattering data from several laboratories[30–34] if we set the hydrodynamic diameter and the persistence length of double helical DNA to be $d = 2.4$ nm and $a = 50$ nm, respectively.

Single-walled carbon nanotubes that are not associated into bundles are also expected to be modeled as wormlike chains.[35–37] Using arguments based on *ab initio* quantum mechanical calculations, Yakobson and Couchman show that the persistence length of defect-free nanotubes with flexibility resulting only from thermal fluctuations is given by $a = Qr^3/T$, where r is the radius of the tube, T is the temperature, and where Q is a material constant of numerical value 7.8×10^7 K nm^{-2} characterizing the inherent flexibility of the graphite sheet.[35] This formula yields, at $T = 300$ K, $a = 9.7$ μm and $a = 11$ μm for (5,5) and for (9,0) nanotubes, respectively, the difference arising from an approximate 4% difference in the radii of the two tubes. Using molecular mechanics calculations and the aromatic-carbon force-field recommended by Boyd et al.,[38] we have obtained very nearly the same result: $a = 11$ μm and $a = 12$ μm, respectively, for (5,5) and for (9,0) defect-free nanotubes.[39] In a calculation employing the Tersoff force-field,[40–42] Buehler obtains $a = 16$ μm for the defect-free (5,5) nanotube.[37] In round numbers, therefore, we will take $a = 10$ μm for the

persistence length of both (5,5) and (9,0) defect-free nanotubes. Interestingly, empirical estimates of the persistence length are much smaller than this. For example, Sano, et al., in measurements of ring-closure probabilities of carbon nanotubes, determine persistence lengths of only 800 nm.[36] However, Yakobson and Couchman assert that the 10 μm estimate, based as it is on first-principles quantum mechanics, must be regarded as accurate for defect-free nanotubes. They attribute the discrepancy to physical or chemical degradation of the tubes.[35] This seems reasonable: Either a sonication vigorous enough to fracture a tube into many pieces or acid etching strong enough to alter its solubility probably inflicts additional damage to the remaining intact pieces. The radius of these two tubes is about 0.34 nm at the atomic centers, while the van der Waals radius of carbon atoms is about 0.16 nm. Therefore, we can estimate the hydrodynamic diameter of these nanotubes to be $d \approx 2 \times (0.34\ \text{nm} + 0.16\ \text{nm}) \approx 1.0$ nm, although this should be regarded as a lower bound in the frequently encountered cases of nanotubes which have been rendered soluble by surface adsorption or modification.

Throughout this paper, we will give interpretations of our results for both double helical DNA and for nanotubes where we take $(d, a) = (2.4\ \text{nm}, 50\ \text{nm})$ for DNA, $(d, a) = (1.0\ \text{nm}, 800\ \text{nm})$ for nanotubes that we assume have been damaged through pretreatment, and $(d, a) = (1.0\ \text{nm}, 10\ \mu\text{m})$ for defect-free nanotubes. We hope that our results will provide a characterization tool to better understand the effects of pretreatment on the persistence length, and therefore on the physical and chemical properties, of nanotubes. Our results can be expected to apply not only to the transport properties of nanotubes in solution, but also to the electrical conductivity of suspensions of conducting nanotubes through the dependence of eq 3 on the intrinsic conductivity. Indeed, conductivity measurements on nanotubes suspended in a polymer matrix should provide an attractive approach for nanotube characterization.

We now outline the remainder of the paper. In section 2, we discuss the freely rotating chains that are used here to model the wormlike chain. In section 3, we present the results of Monte Carlo integrations of the volume and the radius of gyration of wormlike chains; these computations indicate when excluded volume interactions become important for the wormlike chain. Section 4 presents results for the capacity and polarizability in the rod limit. In section 5, we present results for the capacity and polarizability in general, and provide Padé approximants that are good representations of our integration data. In section 6, we compare our results with the calculations of Yamakawa and Fujii.[7,8] We compare our results to empirical data on DNA fractions in section 7, and in section 8, we apply the Padé approximants from section 5 to estimate the "Flory−Fox" parameter, a scale-invariant ratio of the intrinsic viscosity and the cube of the gyration radius. In section 9, we examine the Mark−Houwink behavior of wormlike chains, focusing primarily on how the Mark−Houwink index reflects chain stiffness, and we predict Mark−Houwink indices of both DNA and nanotubes, and finally, we summarize and draw some conclusions in section 10.

2. The Wormlike Chain Model

The wormlike chain model represents a linear polymer as an ensemble of continuous and differentiable space curves. The ensemble contains curves of total contour length L and exhibits tangential correlations of the form[1,2]

$$\langle \mathbf{s}_1 \cdot \mathbf{s}_2 \rangle = \exp\left(\frac{-|s_1 - s_2|}{a}\right) \tag{4}$$

Here $\mathbf{s_1}$ and $\mathbf{s_2}$ are unit tangent vectors at the contour points s_1 and s_2, respectively, and a is the "persistence length." An

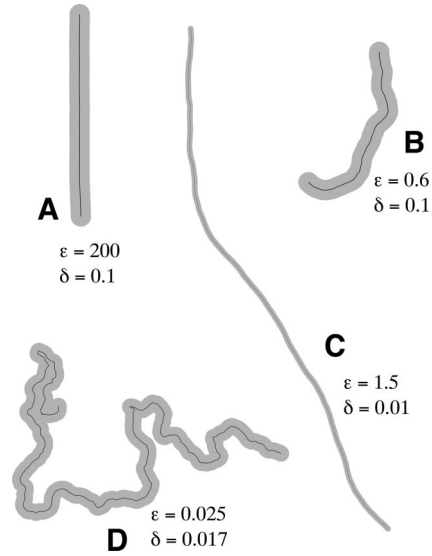

Figure 1. Several realizations of wormlike chains, illustrating how aspect ratio and flexibility vary with the parameters δ and ϵ.

integration of eq 4 leads to the following expression for the "Flory radius," R_F, or rms end-to-end distance:

$$\frac{R_F^2}{L^2} = 2\epsilon - 2\epsilon^2\left[1 - \exp\left(\frac{-1}{\epsilon}\right)\right] \tag{5}$$

where L is the total contour length of the chain and where $\epsilon = a/L$. As a changes relative to L, the model covers the complete range of chain flexibility from rigid rods ($\epsilon \gg 1$) to random coils ($\epsilon \ll 1$). Equation 4 is occasionally taken as the definition of the wormlike chain, but in fact, one can construct many different ensembles all satisfying eq 4 but having different transport properties.[43] The appropriate definition of the wormlike chain model, therefore, is that it is the ensemble of space curves that are the limit sets of freely rotating chains of n steps, of step length l, and of supplementary bond angle θ in the limit that $n \to \infty$, $l \to 0$, and $\theta \to 0$ simultaneously, subject to the constraints that $nl = L$ and $2l/\theta^2 = a$.[1] Obviously, in our integrations, it is impossible to take $n \to \infty$, so we work with freely rotating chains of finite n, but with θ as close to 0 as practically possible. It is well appreciated that transport properties of slender bodies are sensitive to the diameter of the body, so any treatment of the transport properties of wormlike chains must include a third length scale, namely the diameter of the chain, d. For the purposes of our calculations, therefore, we will define a wormlike chain to be the volume swept out by a sphere of diameter d as its center is translated along the contour of a freely rotating chain. Each chain in the ensemble can be thought of as a union of n "sausages," each sausage consisting of the volume swept out by the sphere along one bond of the freely rotating chain. Any particular ensemble is characterized by four variables: n, l, θ, and d, taken as close to the limit $(n, \theta^2, l) \to (\infty, 2L/na, L/n)$ as is practical. All properties are reported as functions of two reduced variables: ϵ and $\delta = d/L$. Figure 1 displays realizations of the model at several different values of ϵ and δ.

There are two practical constraints on our construction of model chains. First, the freely rotating chain does not resemble the wormlike chain if θ is not very close to 0. We regard $\theta \leq 4°$ as preferable, $\theta \approx 5°$ as tolerable, but θ exceeding 5 or 6° as unacceptable. Second, the computations become excessively time-consuming if n becomes much larger than about 10 000. Since $n\theta^2 \to 2/\epsilon$, it is easy to satisfy both constraints for large ϵ, but not for small. Our calculations, therefore, are restricted to $\epsilon \geq 0.025$, which still gives contour lengths equal to 40

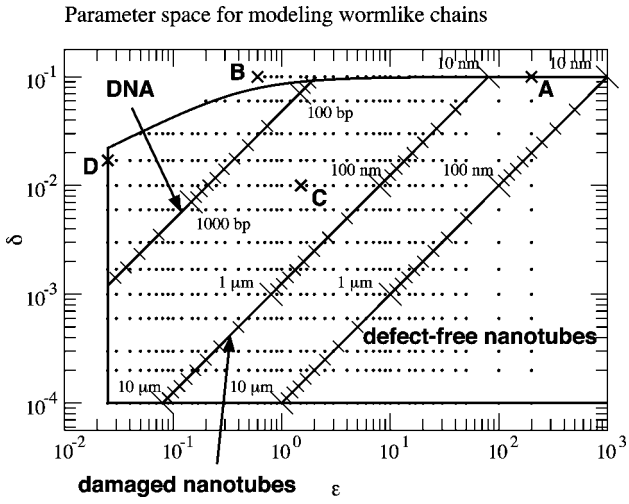

Figure 2. The wormlike chain model involves a two-dimensional parameter space, each point corresponding to a specific aspect ratio, δ, and stiffness, ϵ. Path-integrations were carried out at each of the indicated points. Also shown are lines corresponding to the set of points traced out by DNA and by carbon nanotubes of variable length. Tic marks along the DNA line give the length of the double helix in base pairs. The line labeled "defect-free tubes" corresponds to theoretical defect-free carbon nanotubes. The line labeled "damaged tubes" corresponds to nanotubes whose empirical persistence lengths are much smaller than the theoretical limit, an effect which we believe is attributable to damage via pretreatment. Tic marks along both of the nanotube lines give contour lengths of the tube. The four points designated A, B, C, and D correspond to the four models shown in Figure 1.

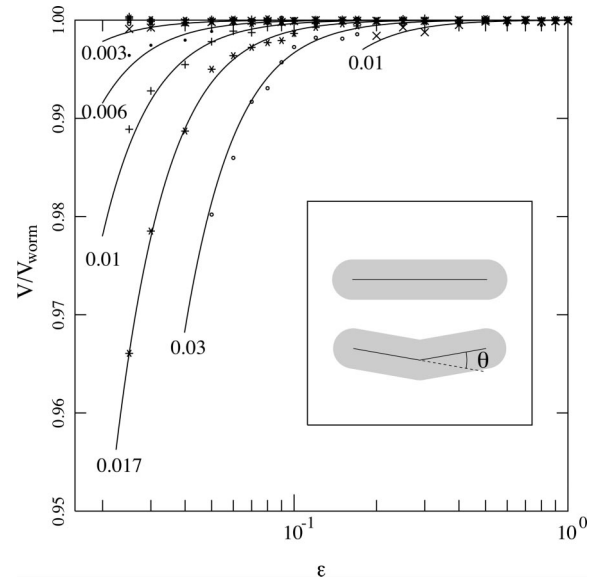

Figure 3. Ratio of the actual volume to that predicted in Eq. 13. Each solid curve is calculated according to eqs 14 and 15 at the displayed values of δ. Deviations away from unity indicate the importance of excluded volume. Inset: The volume of a once-bent rod equals the volume of a straight rod of the same diameter to second order in θ. As shown in the text, this implies that, except for self-excluded volume, a wormlike chain has the same volume as a straight rod of the same length and diameter.

persistence lengths and at least approaches the random coil limit. We also spanned 3 orders of magnitude in the value of δ: $0.0001 \le \delta \le 0.1$. To avoid the extreme in which a sphere translates along a path smaller than the sphere itself, we take any chain for which d is within an order of magnitude of R_F or larger as unrealistic. Therefore, we only consider parameter-space points satisfying $R_F \ge 10d$,

$$2\epsilon - 2\epsilon^2\left[1 - \exp\left(\frac{-1}{\epsilon}\right)\right] \ge 100\delta^2 \tag{6}$$

In the limit of large and small ϵ, this becomes $\delta \le 0.1$ and $\delta \le (\epsilon/50)^{1/2}$, respectively. Figure 2 shows the parameter-space bounded by the inequalities $0.025 \le \epsilon$, $10^{-4} \le \delta \le 10^{-1}$, and eq 6. The straight line labeled "DNA" in Figure 2 consists of the series of points that correspond to $(d, a) = (2.4\text{ nm}, 50\text{ nm})$ for variable L, and spans DNA molecules of total length between about 70 and 6000 base pairs. Similar lines for carbon nanotubes are also shown. The lines labeled "defect-free nanotubes" and "damaged nanotubes" correspond respectively to $(d, a) = (1.0\text{ nm}, 10\ \mu\text{m})$ and $(d, a) = (1.0\text{ nm}, 800\text{ nm})$ and span tubes of total length between 10 nm and 10 μm.

Excluded volume interactions become important at small ϵ and eventually invalidate the wormlike chain model. We show below that the translating sphere sweeps equal volume whether its trajectory is a straight line or a wormlike curve, but of course, intersections of the chain with itself can lead to multiple counting of some regions of space. We compare the average volume swept out by the sphere to the volume swept out by the same sphere translating along a straight line, and regard the model as compromised by excluded volume interactions whenever the two differ. We use a Monte Carlo integration to determine V, and the same integration also permits us to estimate R_g with no additional effort. We evaluated C, $\langle\alpha\rangle$, V, and R_g at a total of 553 unique parameter-space points, shown in Figure 2, and report our results below. At each point in parameter-space, we generated 10^4 representative chains, performed the path-integration on each one of these, and performed ensemble averages as described elsewhere.[29]

3. Volume and Radius of Gyration of Wormlike Chains

An appropriate integration of eq 4 gives the following formula for the radius of gyration, exact in the "slender worm" limit $\delta \to 0$:[2]

$$\frac{R_{g,thin}^2}{L^2} = \frac{\epsilon}{3} - \epsilon^2 + 2\epsilon^3 - 2\epsilon^4\left[1 - \exp\left(\frac{-1}{\epsilon}\right)\right] \quad (\delta \to 0) \tag{7a}$$

Computations based directly on eq 7a are numerically unreliable at large ϵ, because of the cancelation of several large terms. For $\epsilon > 10$, therefore, we recommend the following series expansion of eq 7a:

$$\frac{R_{g,thin}^2}{L^2} = \sum_{k=0}^{\infty} \frac{2}{(k+4)!}\left(\frac{-1}{\epsilon}\right)^k \quad (\delta \to 0) \tag{7b}$$

It is also trivial to determine exact expressions for the radius of gyration and the volume in the rod limit $\epsilon \to \infty$:

$$\frac{R_{g,rod}^2}{L^2} = \frac{1 + 2\delta + 3\delta^2 + \frac{6}{5}\delta^3}{12 + 8\delta} \quad (\epsilon \to \infty) \tag{8}$$

$$\frac{V_{rod}}{L^3} = \frac{\pi\delta^2}{4} + \frac{\pi\delta^3}{6} \quad (\epsilon \to \infty) \tag{9}$$

Equations 8 and 9 give the exact finite-δ corrections to the well-known limiting forms $R_g^2 = L^2/12$ and $V = 0$.

We next consider the volume swept out by a sphere of radius $R = d/2$ when it translates along only two bonds of a freely rotating chain. (Figure 3) The volume in that case proves to be given by $V_{rod} + V_{bend}$ where V_{rod} is the volume swept out by the same sphere following a straight trajectory (given by eq 9) and

$$V_{bend} = -\frac{4\pi}{3}R^3F(\theta) \tag{10}$$

where

$$F(\theta)=\frac{1}{\pi}\left[\tan\left(\frac{\theta}{2}\right)-\frac{\theta}{2}\right]\cong\frac{\theta^3}{24\pi} \tag{11}$$

Defined in this way, V_{bend} can be regarded as the contribution of the bend to the total volume. Note that it is negative, and scales as θ^3 when θ is small. It follows that if we incorporate n bends in a chain, then the change in volume is

$$\Delta V=-\frac{4\pi}{3}R^3F(\theta)n\sim n\theta^3 \tag{12}$$

In the wormlike limit, since $n\theta^2=2/\epsilon$ is constant, then $n\theta^3\rightarrow 0$. Therefore, by this argument, the wormlike chain has the same volume at any value of ϵ, independent of chain flexibility:

$$\frac{V_{\text{worm}}}{L^3}=\frac{\pi\delta^2}{4}+\frac{\pi\delta^3}{6} \tag{13}$$

However, as already mentioned, eq 13 neglects the fact that the chain can pass through itself, especially for small ϵ. Total volumes smaller than eq 13 are indicative of self-intersections. Figure 3 shows our calculated values of V/V_{worm} as functions of ϵ for each given value of δ. Observe that this ratio is very near 1 except at small ϵ, and never more than a few percent less than 1 in all regions of the parameter space that we examined. We have been able to successfully represent all of the volume data in terms of a single master curve (not shown). If we plot V/V_{worm} as a function of the variable,

$$r_V=\epsilon\delta^{-0.771} \tag{14}$$

then all points fall on a curve that is represented acceptably by the following Padé approximant:

$$\frac{V}{V_{\text{worm}}}=\frac{1+(0.004898){r_V}^{-1.841}}{1+(0.01414){r_V}^{-2.27}} \tag{15}$$

Each of the solid curves appearing in Figure 3 was drawn using eqs 14 and 15. As is obvious in Figure 3, eq 15 has an uncertainty of about one part in one thousand. The coefficients and exponents in eq 15 were determined by simulated annealing.[44] Given that V/V_{worm} is within a few percent of unity, we conclude that excluded volume interactions are relatively unimportant in all regions of parameter space that we examined. However, they undoubtedly become significant at still smaller ϵ.[45] Figure 4 displays a contour plot that shows the dependence of V/V_{worm} as calculated by eqs 14 and 15 on ϵ and δ, and also lets us judge the strength of excluded volume interactions for both DNA double helices and carbon nanotubes.

Equations 7 and 8 are both correct representations for the gyration radius of the wormlike chain in the respective limits $\delta\rightarrow 0$ and $\epsilon\rightarrow\infty$. As can be seen in Figure 5, the following renormalized product of the two gives an accurate representation of our R_g data over the entire range studied:

$$\frac{R_g}{L}=\frac{\sqrt{12}R_{g,\text{thin}}R_{g,\text{rod}}}{L^2} \tag{16}$$

Therefore, eq 16 represents the finite-thickness correction to eq 7. Interestingly, eq 7 is usually considered to be adequate for all wormlike chains. However, as Figure 5 shows, these finite-thickness corrections are necessary in the rod limit as δ approaches 0.1. In Figure 6, we display a contour plot of the dependence of R_g/L on ϵ and δ calculated according to eq 16.

4. Results for the Capacity and Polarizability in the Rigid-Rod Limit

The wormlike chain in the rod-limit is the body swept out by a sphere of radius d translating along a straight line of length L. Miles has derived the following expressions for the electrostatic properties of rigid rods with circular cross-section:[46]

$$\frac{C_{\text{rod}}}{L}=\frac{1}{2}(1+\delta)[\ln u+\ln 4-1]^{-1} \tag{17}$$

$$\frac{\langle\alpha\rangle_{\text{rod}}}{L^3}=\frac{\pi}{18}(1+\delta)^3\left[\ln u+\ln 4-\frac{7}{3}\right]^{-1} \tag{18}$$

where

$$u=\frac{L+d}{d}=\delta^{-1}+1 \tag{19}$$

These are only asymptotically correct in the limit $\delta\rightarrow 0$, but the following two formulas are very accurate expressions for C and $\langle\alpha\rangle$ for rigid rods in the range $10^{-4}\le\delta\le 10^{-1}$, and were obtained by fitting polynomials in $(\ln u)^{-1}$ to the

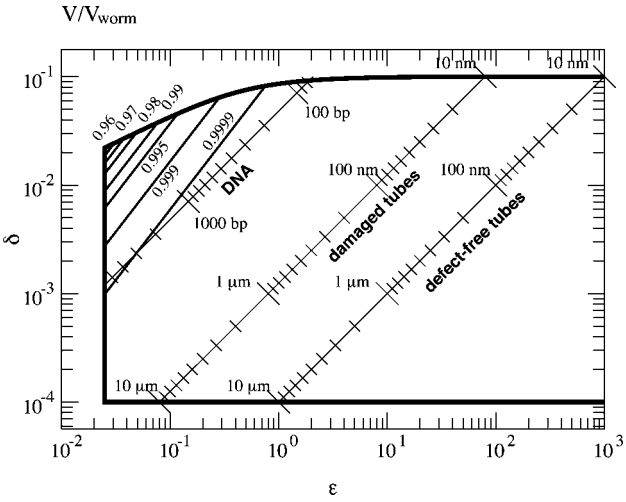

Figure 4. Contour plot showing the variation of V/V_{worm} throughout the parameter space. The three lines corresponding to DNA and to nanotubes are the same as those from Figure 2.

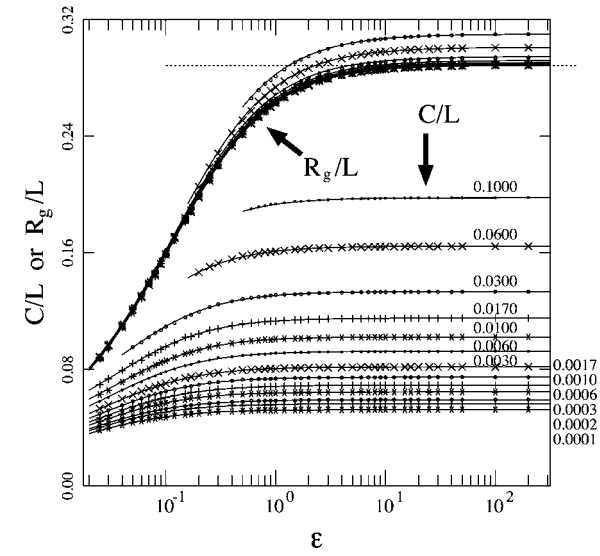

Figure 5. Integration data for gyration radii and capacities, normalized by the length and displayed as functions of ϵ. Symbols are the integration results. Solid curves for R_g/L are calculated according to eqs 7, 8, and 16 at (reading from the top) $\delta=0.1$, 0.06, 0.03, 0.017, 0.01,..., 0.0001. Whenever $\delta<0.01$, however, individual R_g/L curves are unresolvable. The dashed curve lies at $R_g/L=(12)^{-1/2}$, the asymptotic value for thin, straight rods. Solid curves for C/L were drawn using eqs 20, 22, and 24. Each is labeled with a value of δ.

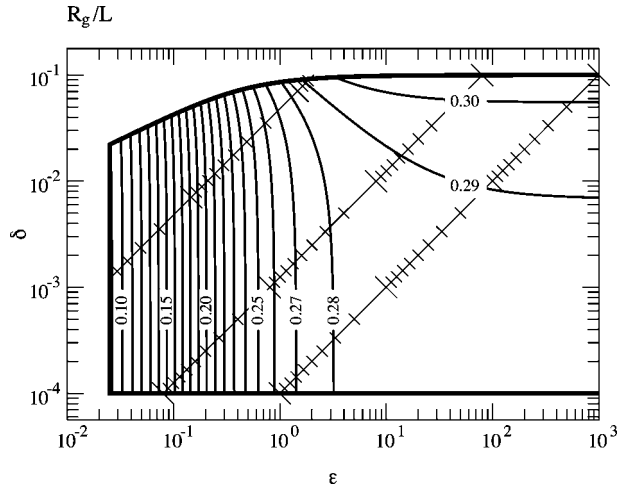

Figure 6. Contour plot giving R_g/L as a function of δ and ϵ. The lines for DNA and for nanotubes have been transferred from Figure 2, although in this and subsequent figures, the labels on the lines are omitted for clarity.

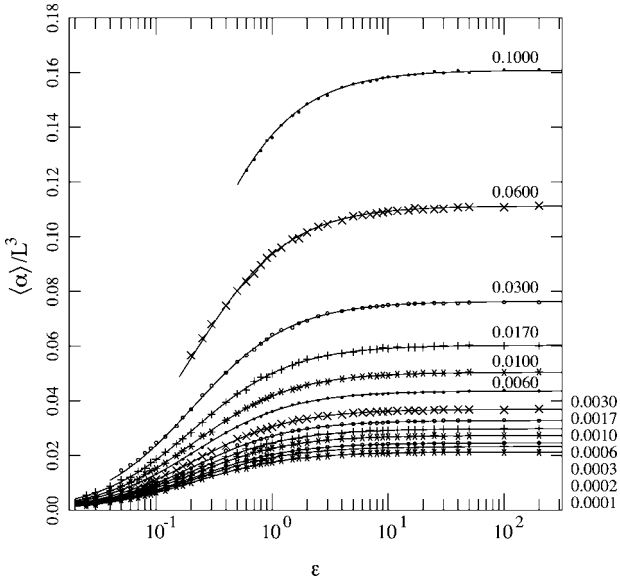

Figure 7. Integration results for the mean polarizability. Individual symbols are the raw integration results. Solid curves were drawn using eqs 21, 23, and 25. Each is labeled with a value of δ.

residuals obtained between eqs 17 and 18 and the raw integration data.

$$\frac{C_{\text{rod}}}{L} = \frac{1}{2}(1+\delta)[\ln u + \ln 4 - 1 - \frac{3.95}{(\ln u)^2} + \frac{16.18}{(\ln u)^3} - \frac{16}{(\ln u)^4}]^{-1} \tag{20}$$

$$\frac{\langle\alpha\rangle_{\text{rod}}}{L^3} = \frac{\pi}{18}(1+\delta)^3\left[\ln u + \ln 4 - \frac{7}{3} - \frac{4.53}{(\ln u)^{1.72}} + \frac{18.3}{(\ln u)^{2.72}} - \frac{18}{(\ln u)^{3.72}}\right]^{-1} \tag{21}$$

Since these formulas also tend to the Miles asymptotic formulas as $\delta \to 0$, they should also be reliable for any values of δ less than 10^{-4}. In another publication,[47] we give other Padé approximants for C_{rod} and $\langle\alpha\rangle_{\text{rod}}$, which cover a broader range of δ, but which also contain more terms. In this paper, because we restrict ourselves to δ below 0.1, the above approximants are adequate.

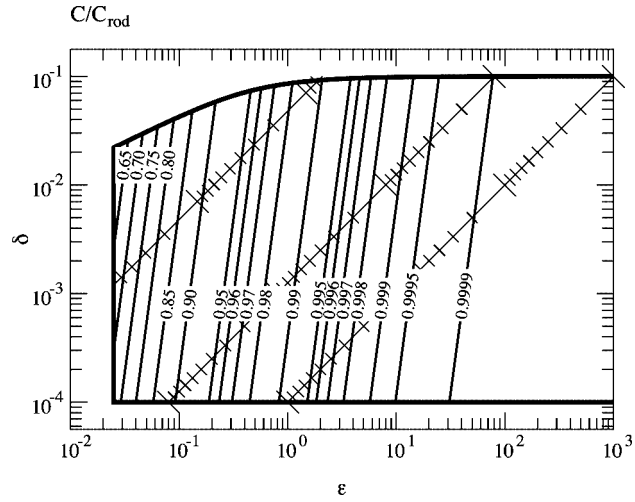

Figure 8. Contour plot showing C/C_{rod} as a function of ϵ and δ, drawn using eqs 22 and 24.

5. Results for the Capacity and Polarizability of Wormlike Chains

Integration results for the capacity and the mean polarizability appear in Figures 5 and 7. Notice that the curves level off as ϵ increases, which of course represents convergence to the rod limit. These curves also indicate the sensitivity of the electrostatic and transport properties to the diameter of the rod, since we observe δ-dependence even when δ becomes extremely small.

Much like the volume data discussed above, we have also been able to reduce the electrostatic data to universal curves. A vertical shift, achieved by dividing each data-point by its corresponding value in the rod limit, eqs 20 or 21, followed by a horizontal shift, superimposes the individual curves. The data can be reduced to dependence on the following two variables:

$$r_C = \epsilon\delta^{-0.134} \tag{22}$$

$$r_\alpha = \epsilon \exp[(3.106)\delta^{1.213}] \tag{23}$$

The master curves can be represented by the following Padé approximants,[44] again obtained by simulated annealing:

$$\frac{C}{C_{\text{rod}}} = \frac{1+(0.03801)r_C^{-0.9212}}{1+(0.07204)r_C^{-1.0204}} \tag{24}$$

$$\frac{\langle\alpha\rangle}{\langle\alpha\rangle_{\text{rod}}} = \frac{1-(0.005690)r_\alpha^{-0.8350}}{1+(0.2028)r_\alpha^{-1.0335}} \tag{25}$$

The solid curves shown in Figures 5 and 7 were drawn using eqs 20–25. The results of eqs 20–25 are also shown in Figures 8 and 9, which are contour plots of the dependence of C/C_{rod} and of $\langle\alpha\rangle/\langle\alpha\rangle_{\text{rod}}$ on ϵ and δ. Once C and $\langle\alpha\rangle$ have been determined at any given value of ϵ and δ, we use eqs 1–3 to compute either the hydrodynamic radius or the intrinsic viscosity.[23] Figures 5, 7, 8, and 9 demonstrate, among other things, that, over the parameter space that we considered, the capacity drops to about 60% or 70% of its value in the rod limit, while the polarizability drops to below 10% of its rod value.

6. Comparison with Previous Transport Property Calculations

The most extensive, previous calculations of the hydrodynamic radius and the intrinsic viscosity of wormlike chains of which we are aware are the work of Yamakawa and Fujii.[7,8] They employed orientational preaveraging, or the "electrostatic

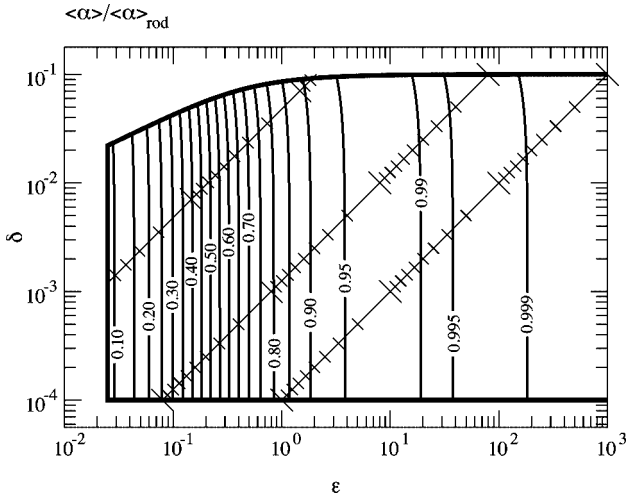

Figure 9. Contour plot showing $\langle\alpha\rangle/\langle\alpha\rangle_{rod}$ as a function of ϵ and δ, drawn using eqs 23 and 25.

approximation," but they made several other approximations as well, obtaining integral equations that they then solved numerically. They also gave least-squares fitted formulas to represent their numerical results. We show below that the Yamakawa−Fujii theory is accurate for long chains, but there are some inaccuracies when the chains become short. This difficulty can be traced to the description of the polymer chain as hydrodynamic point sources (or hydrodynamic "beads"), which in some circumstances can be problematic.[25] A precise analysis of these slender-body approximation errors has been made by Goren and O'Neill[48] for the particular case of cylinders wrapped into rings (i.e., toroids) where they compare their *exact* hydrodynamic computations to those of hydrodynamic bead models. Goren and O'Neill find that the error of Yamakawa and Fujii derive from the slender body or "bead" approximation, as applied to relatively compact polymers. In previous work, we have shown that our path-integral method gives highly accurate results for the torus. In particular, we obtain results that are accurate for the friction coefficient to better than 1% in the regime where the Yamakawa−Fujii estimates become problematic. Recently, we have found deviations of a similar magnitude in previous bead computations of short cylinders, [47] and other models.[25] We show below, however, that the errors of the slender-body approximation become small in the limit of long chains.

Figures comparing our predictions with the Yamakawa−Fujii results are given in the Supporting Information accompanying this paper. We find that the Yamakawa−Fujii estimates for the hydrodynamic radius agree well with our estimates throughout much of the parameter space. Nevertheless, their estimates for the hydrodynamic radius are approximately 25% too high in the rod limit as we approach $\delta = 0.1$, and about 10% too low in the vicinity of $\epsilon = 0.025$ and $\delta = 0.02$ (the extreme upper left of Figure 2). These discrepancies are evidently due to the bead approximation, as noted above.

For the $\langle\alpha\rangle$ data, there is reasonable agreement between the two sets of formulas over much of the parameter space, but not when we approach $\delta = 0.1$ in the rod limit, where we observe discrepancies approaching 15%. Discrepancies are also apparent as we approach the coil limit where ϵ is small.

7. Comparisons with Empirical Data on DNA

If the wormlike chain model is a valid representation of native double-helical DNA, then it should be possible to assign unique model parameters a and d that apply at any L and in any experiment. A number of previous attempts[30–33] at interpreting transport properties of DNA to obtain such model parameters have employed the Yamakawa-Fujii calculations.[7,8] However, as can be seen in the Supporting Information, the Yamakawa−Fujii calculations can be in error by as much as 15% or 20%, especially for short DNA chains. Therefore, it is timely to analyze available DNA data using our new results.

Table 1. Empirical Data on DNA Fractions

source ref	M_n (kg/mol)	n (bp)	L (nm)	M_w/M_n	s (Sv)	$[\eta]_P$(L/g)	R_h (nm)	R_g (nm)	$\langle\alpha\rangle^{1/3}$ (nm)
32	1150	1735	590	1	10.78		43.0		
32	1060	1606	546	1	10.67		40.2		
32	869	1310	445	1	9.99		35.0		
30, 31	780	1176	400	1.11	9.54	0.582	32.9	78.4	98.5
30, 31	632	953	324	1.05	9.01	0.469	28.3	64.3	85.4
32	565	854	290	1	8.72		26.2		
32	526	794	270	1	8.59		24.7		
30, 31	522	787	268	1.05	8.60	0.366	24.5	58.2	73.8
30, 31	446	673	229	1.05	8.18	0.292	22.0	48.7	64.9
32	426	642	218	1	8.03		21.4		
32	392	592	201	1	7.89		20.1		
30, 31	360	543	185	1.02	7.67	0.232	18.9	40.9	56.0
33	340	513	174	1.29		0.241		57.4	55.6
32	330	498	169	1	7.62		17.5		
34	293	442	150	1.36		0.234			52.4
34	285	430	146	1.27		0.222			51.0
30, 31	273	412	140	1.03	7.16	0.152	15.4	34.6	44.3
32	213	322	109	1	6.70		12.8		
34	204	308	105	1.25		0.157			40.7
32	191	288	98	1	6.37		12.1		
33	191	288	98	1.29		0.165		40.1	40.5
32	174	263	89	1	6.24		11.3		
33	152	229	78	1.18		0.115		31.9	33.2
34	132	199	68	1.25		0.089			29
33	131	198	67	1.08		0.087		26.3	29
32	106	160	54	1	5.41		7.9		
32	96	145	49	1	5.20		7.5		
33	78	118	40	1.06		0.029		16.4	17
32	78	117	40	1	4.92		6.4		
34	63	96	33	1.20		0.030			16
32	62	94	32	1	4.58		5.5		
32	33	50	17	1	3.51		3.8		

We have extracted data from four different sources: (1) Godfrey and Eisenberg[30,31] publish sedimentation, viscosity, and light scattering results on DNA fractions prepared by sonication and fractionated by ultracentrifugation. (2) Kovacic and van Holde[32] give sedimentation results for DNA fractions prepared by restriction enzyme digestion. (3) Fukudome et al.[33] present viscosity and light scattering results on fractions prepared by sonication and fractionated by successive precipitation. (4) Tanigawa et al.[34] provide viscosity data on fractions also prepared by sonication and successive precipitation. Of the various preparation and fractionation techniques, restriction enzyme digestion affords the narrowest molecular weight distributions, followed by ultracentrifugation, and then by successive precipitation. Therefore, the Kovacic−van Holde samples are effectively monodisperse, while the Godfrey−Eisenberg samples also have relatively narrow distributions, with reported polydispersities generally below 1.1. The remaining two sample sets have larger polydispersities, sometimes exceeding 1.3.

Because a careful analysis requires samples that are as monodisperse as possible, we have rejected data on any samples with reported polydispersities greater than 1.3 or for which polydispersities are not reported. All molecular weights (and equivalently contour lengths and numbers of base pairs) used in our analysis are number-average, and we rejected any samples for which the number-average was not available. We have extracted R_h values from sedimentation data using the well-known sedimentation equation

$$s = \frac{M(1-\bar{v}\rho)}{6\pi\eta N_A R_h} \tag{26}$$

where s is the sedimentation coefficient, M is the molecular weight, η is the solvent viscosity, N_A is Avogadro's number,

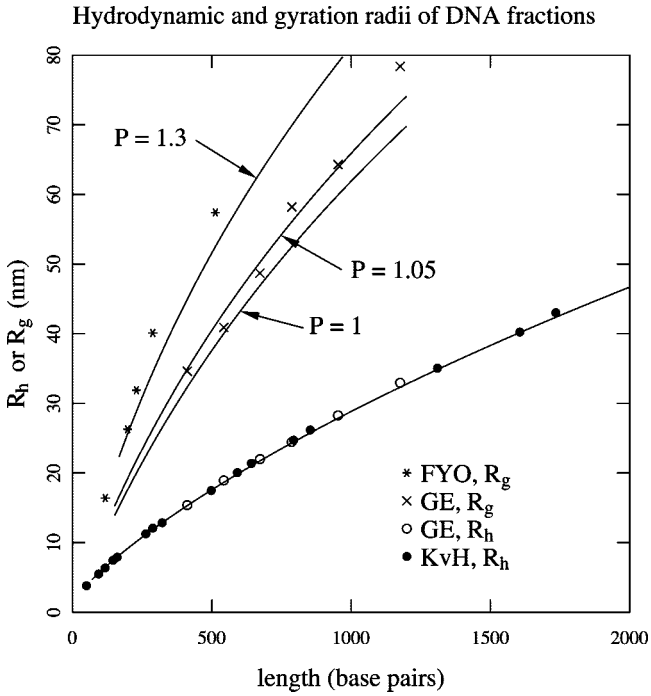

Figure 10. Comparison between experimental values (symbols) and predictions (solid curves) of the hydrodynamic radius and gyration radius of DNA fractions. Experimental values are from sedimentation data of Kovacic and van Holde.[32] (KvH), sedimentation and light scattering data of Godfrey and Eisenberg[30,31] (GE), and light scattering data of Fukudome et al.[33] (FYO). Our predictions are drawn assuming d (diameter) = 2.4 nm and a (persistence length) = 50 nm. Our predictions for the root-z-average-square radius of gyration are for fractions of the indicated polydispersity, $P = M_w/M_n$, assuming molecular mass distributions described in the text.

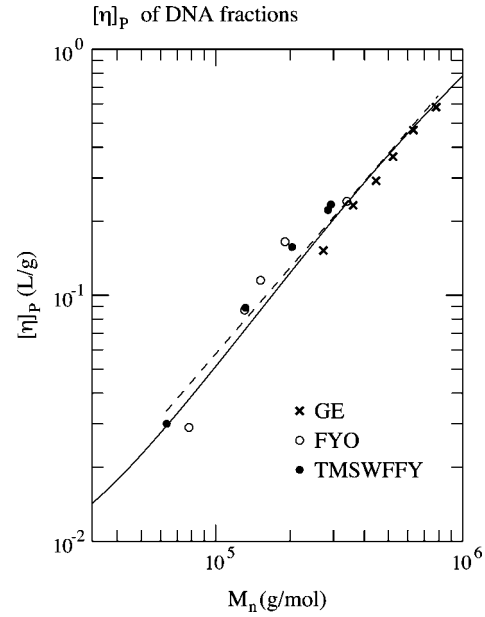

Figure 11. Comparison between experimental intrinsic viscosity data on DNA fractions, obtained from Godfrey and Eisenberg[30,31] (GE), Fukudome et al.[33] (FYO), and Tanigawa, et al.[34] (TMSWFFY), and the predictions of our calculations, drawn assuming d (diameter) = 2.4 nm, and a (persistence length) = 50 nm. The dashed line is the linear-least-squares fit to the experimental data and has slope 1.17.

and $(1 - \bar{v}\rho)$ is the buoyancy factor. We work directly with published sedimentation coefficients corrected to 20 °C in water, for which $(1 - \bar{v}\rho)/\eta = 4.58 \times 10^{21}$ Sv·nm·g^{-1}.[32] We take the molecular mass per base pair to be M/n = 663 g·mol^{-1}·bp^{-1}, where n is the length of the molecule in base pairs (bp), and we take the contour length per base pair to be L/n = 0.340 nm·bp^{-1}. Table 1 and Figures 10 and 11 summarize the data used in our analysis.

Light scattering measures the z-average square radius of gyration, which is obviously very sensitive to polydispersity. This sensitivity is obvious in Figure 10, where gyration radius data obtained on the sonication/precipitation fractions lie on a curve distinct from those obtained on the sonication/ultracentrifugation fractions. Therefore, to avoid distortions, we base our determination of a and d only on the transport data, which are generally less sensitive to polydispersity. The model parameters a and d were determined by minimizing the following least-squares function:

$$S(a,d) = \sum_i w_i \left[1 - \frac{r_{pi}(a,d)}{r_{xi}}\right]^2 \tag{27}$$

Here, r_{xi} is one of the experimental measurements (either a value of R_h or of $\langle\alpha\rangle^{1/3}$) appearing in Table 1, with the index i ranging over all data points, and $r_{pi}(a,d)$ is our prediction for the same parameter. To further avoid biases generated by polydispersity, we have assigned weight factors of $w_i = 2$ to data from refs 30–32 and $w_i = 1$ to data from refs 33 and 34. We have chosen to base the minimization on $\langle\alpha\rangle^{1/3}$ rather than $[\eta]_P$, because $\langle\alpha\rangle^{1/3}$ is a length and therefore on a more equal footing with R_h. We determined the model values which minimize eq 27, d = 2.4 nm and a = 50 nm, by a grid search. These model values are consistent with earlier determinations.[30–33,49–53] Figures 10 and 11 show the quality of fit between the model and the data for R_h and $[\eta]_P$. Figure 10 shows three different curves for the root-z-average-square radius of gyration, plotted according to our model with d = 2.4 nm and a = 50 nm, but assuming a molecular mass distribution of the indicated polydispersity. The curves in Figure 10 for R_g were plotted assuming a Gaussian distribution of molecular weights (but truncated at zero molecular weight) with peak and half-width adjusted to give the indicated number-average molecular mass and polydispersity. Although one might hope for better accord between these curves and the experimental data, we should bear in mind that the precise molecular weight distribution is unknown and that the polydispersity varies from sample to sample. Therefore, these curves indicate that the disparity between the R_g data from the two laboratories is attributable to polydispersity, and that unique values of d and a are able to account for the results of all three classes of experiments.

We have contemplated performing a more careful analysis of the data in Table 1, one in which each data-point is corrected for polydispersity. But more useful would be careful experimental results on restriction enzyme digests, and we encourage experimentalists to provide such data.

Obviously, our computations neglect counterion dissipation effects which can be important to the transport properties of polyelectrolytes such as DNA.[50–54] Presumably, these are unimportant at the physiological salt concentrations employed in these experiments. The ability to fit the data to our results supports this assumption.

8. Flory−Fox Parameter of Wormlike Chains

The Flory−Fox parameter is the following ratio

$$\Phi = \frac{m[\eta]_P N_A}{(6^{1/2}R_g)^3} \tag{28}$$

Since it is scale-invariant it serves as a convenient signature of particle shape obtained by combining the results of two separate observations on the same particle. Figure 12, calculated using eqs 7, 8, 16, 21, 23, and 25, shows how Φ varies throughout our parameter space. The generally accepted value of Φ for

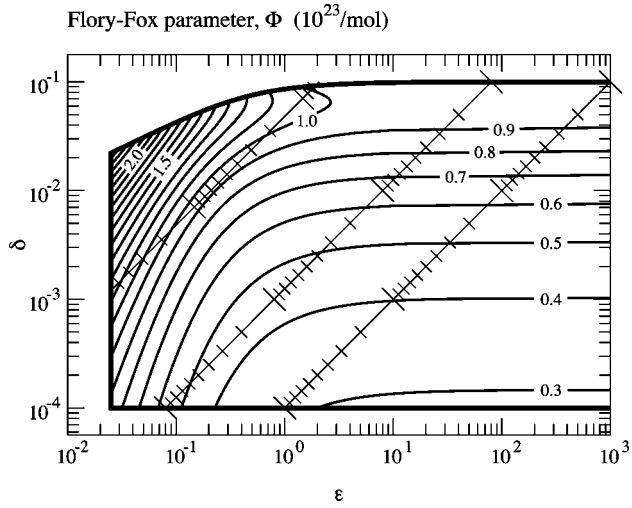

Figure 12. Flory−Fox parameter Φ of wormlike chains as a function of ϵ and δ.

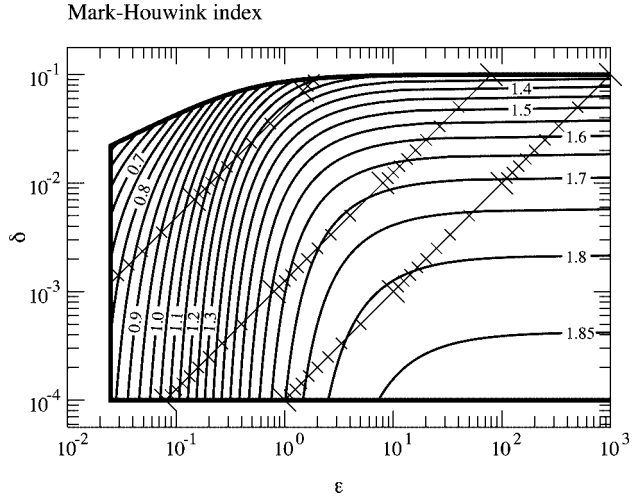

Figure 13. Mark−Houwink index of wormlike chains as a function of ϵ and δ.

θ-state coils is in the range (2.5−2.7) × 10^{23} mol^{-1}, to which our results are seen to converge when ϵ is small. This plot also indicates that chain stiffness leads to values lower than this limit. It also indicates that the ratio depends on rod diameter in the rod limit.

9. Mark−Houwink Behavior

A well-known empirical relationship between molecular weight and intrinsic viscosity is the Mark−Houwink law:

$$[\eta]_P = KM^{\beta} \tag{29}$$

The exponent β is often molecular weight dependent, but it usually varies weakly enough that it can be regarded as constant, sometimes even over relatively broad molecular weight ranges. Its value is another signature of the conformation of the macromolecule. For random coils, it varies between about 0.5 and 0.77, depending on solvent quality. For chains that are stiff enough that excluded volume becomes irrelevant it no longer indicates solvent quality, but it still reflects chain stiffness. In this section, we consider how β varies throughout the parameter space of the wormlike chain. We assume that M is proportional to V_{worm}, and take

$$\beta = \frac{\partial(\ln [\eta]_P)}{\partial(\ln V_{worm})} = \frac{V_{worm}}{[\eta]_P}\left[\frac{\partial [\eta]_P}{\partial L}\right]_{a,d}\left[\frac{\partial V_{worm}}{\partial L}\right]_{a,d}^{-1} \tag{30}$$

We then assume that $[\eta]_P$ is given by eqs 2b, 21, 23, and 25 while V_{worm} is given by eq 13. Figure 13 shows the value of β throughout parameter space.

According to Figure 13, β is near 1.3 for DNA samples between about 100 and 400 bp, near 1.2 between about 400 and 700 bp, and near 1.1 between 700 and 1200 bp. The data displayed in Figure 11 cover this same range, and the single best fit line through the data has slope 1.17. For defect-free nanotubes of length around 1 μm, we can expect β values near 1.8, or if the line labeled "damaged" is more realistic, then β is nearer 1.6.

As another example, we consider intrinsic viscosity data on polymeric aromatic amides,[55] where $\beta \approx 1.2$ over a molecular weight range of 1.8 to 18.5 kDa. It is suggested for these polymers that L/d is approximately equal to the degree of polymerization,[55] implying that this molecular weight range corresponds approximately to $0.006 < \delta < 0.06$. Tuning ϵ/δ to give $\beta \approx 1.2$ over this molecular weight range gives $\epsilon/\delta = a/d \approx 20$. In other words, we predict a persistence length of about 20 monomers for these rather stiff polymers.

As a third example, the Mark−Houwink exponent has also recently been discussed as a qualitative characterization parameter for carbon nanotubes.[56] We expect this usage to grow as fractionated samples of carbon nanotubes become available.

10. Conclusions

In this paper, we have applied our numerical path-integration technique to predict the hydrodynamic radius and intrinsic viscosity of wormlike chains. Computations have been performed over as wide a range as possible of the parameter space of the wormlike chain, in which the diameter-to-length ratio, δ, and the persistence-length-to-length ratio, ϵ, constitute the independent parameters. We have represented the results in terms of Padé approximants that permit rapid computation of both the hydrodynamic radius and the intrinsic viscosity of wormlike chains anywhere within the covered parameter space. The approximants give good results at any values of δ and ϵ within the domain shown in Figure 2. Extrapolations beyond that domain should not be trusted, with the exception of the domain $\delta < 10^{-4}$ near the rod limit. An advantage of our method compared to previous methods of computation is that it avoids errors from the bead approximation which can become appreciable in some situations. Our method can also treat arbitrary structures, including random coils and branched polymers. We can thus begin to model the transport properties of polymer chains in a more physically realistic way.

We have also determined the radius of gyration and volume of the same wormlike chain models over the same parameter space by Monte Carlo integration, and supplied Padé approximants to represent those results. The volume results permit us to determine the importance of excluded volume interactions at any particular point in δ−ϵ space. We find, for example, excluded volume interactions are unimportant whenever the persistence-length-to-length ratio exceeds 0.025. The radius-of-gyration results permit us to give finite-thickness corrections to the standard formula for the radius of gyration, which prove to be significant at larger values of δ.

When compared with empirical sedimentation, viscometric, and light scattering data on DNA fractions, our computations predict a diameter and persistence length of 2.4 and 50 nm, respectively, for double helical DNA. Our computations also permit us to estimate the persistence length of a polymeric aromatic amide from viscometric data.

There are significant discrepancies between the theoretical persistence length of defect-free nanotubes and those obtained by experiment. We have made a number of predictions about

the transport properties of single-walled nanotubes, and hope that these results will prove useful in ongoing efforts to characterize these promising materials.

Acknowledgment. The computations reported here were performed using the High Performance Computing Facility of Stevens Institute of Technology.

Supporting Information Available: Figures comparing our predictions against those of Yamakawa and Fujii[7,8] and text discussing this comparison. This material is available free of charge via the Internet at http://pubs.acs.org.

References and Notes

(1) Flory, P. J. *Statistical Mechanics of Chain Molecules*; Wiley: New York, 1969.
(2) Yamakawa, H. *Modern Theory of Polymer Solutions*; Harper & Row: New York, 1971.
(3) Doi, M.; Edwards, S. F. *The Theory of Polymer Dynamics*; Oxford University Press: Oxford, U.K., 1986.
(4) Hearst, J. E.; Stockmayer, W. H. *J. Chem. Phys.* **1962**, *37*, 1425–1433.
(5) Ullman, R. *J. Chem. Phys.* **1968**, *49*, 5486–5497.
(6) Ullman, R. *J. Chem. Phys.* **1970**, *53*, 1734–1740.
(7) Yamakawa, H.; Fujii, M. *Macromolecules* **1973**, *6*, 407–415.
(8) Yamakawa, H.; Fujii, M. *Macromolecules* **1974**, *7*, 128–135.
(9) Yamakawa, H. *Macromolecules* **1975**, *8*, 339–342.
(10) Fujii, M.; Yamakawa, H. *Macromolecules* **1975**, *8*, 792–799.
(11) Shimada, J.; Yamakawa, H. *Macromolecules* **1976**, *9*, 583–586.
(12) Yamakawa, H. *Macromolecules* **1983**, *16*, 1928–1931.
(13) Tanaka, G.; Yoshizaki, T.; Yamakawa, H. *Macromolecules* **1984**, *17*, 767–773.
(14) Hubbard, J. B.; Douglas, J. F. *Phys. Rev. E* **1993**, *47*, 2983–2986.
(15) Zhou, H.-X.; Szabo, A.; Douglas, J. F.; Hubbard, J. B. *J. Chem. Phys.* **1994**, *100*, 3821–3826.
(16) Douglas, J. F.; Zhou, H.-X.; Hubbard, J. B. *Phys. Rev. E* **1994**, *49*, 5319–5331.
(17) Given, J. A.; Hubbard, J. B.; Douglas, J. F. *J. Chem. Phys.* **1997**, *106*, 3761–3771.
(18) Douglas, J. F.; Garboczi, E. J. *Adv. Chem. Phys.* **1995**, *91*, 85–153.
(19) Douglas, J. F. *Adv. Chem. Phys.* **1997**, *102*, 121.
(20) Mansfield, M. L.; Douglas, J. F.; Garboczi, E. J. *Phys. Rev. E* **2001**, *64*, 061401.
(21) Mansfield, M. L.; Douglas, J. F. *Condens. Matter Phys.* **2002**, *5*, 249–263.
(22) Kang, E.-H.; Mansfield, M. L.; Douglas, J. F. *Phys. Rev. E* **2004**, *69*, 031918.
(23) Elsewhere, we have advocated a more precise method (accurate to about 1%) for determining q_η; see ref 29. In principle, it should be possible also to apply this method to the wormlike chain, taking the form of a Padé approximant for q_η in terms of ϵ and δ. However, these wormlike chain computations predated the development of the newer technique for q_η. Therefore, for the time being, when using our wormlike chain approximants, we recommend eq 3 to convert from $\langle\alpha\rangle$ to $[\eta]$. We hope eventually to provide more accurate estimates of q_η for the wormlike chain model.
(24) As evidence of versatility, we site the class of objects that we have successfully treated by this technique: ellipsoids and cylinders over a wide range of aspect ratios, general polyhedra (many having very complex shapes), tori, disks, polygons, proteins, random coil chains and stars, dendrimers, diffusion-limited aggregates, fractal sets, and now, wormlike chains. See refs 20–22 and 25.
(25) Mansfield, M. L.; Douglas, J. F.; Irfan, S.; Kang, E.-H. *Macromolecules* **2007**, *40*, 2575–2589.
(26) Zimm, B. H. *Macromolecules* **1980**, *13*, 592–602.
(27) Fixman, M. *J. Chem. Phys.* **1983**, *78*, 1588–1593.
(28) Fixman, M. *J. Chem. Phys.* **1983**, *78*, 1594–1599.
(29) Mansfield, M. L. ; Douglas, J. F. , Submitted to *Phys. Rev. E.*
(30) Godfrey, J. E. *Biophys. Chem.* **1976**, *5*, 285–299.
(31) Godfrey, J. E.; Eisenberg, H. *Biophys. Chem.* **1976**, *5*, 301–318.
(32) Kovacic, R. T.; van Holde, K. E. *Biochemistry* **1977**, *16*, 1490–1498.
(33) Fukudome, K.; Yamaoka, K; Ochiai, H. *Polym. J.* **1987**, *19*, 1385–1394.
(34) Tanigawa, M; Mukaiyama, N.; Shimokubo, S.; Wakabayashi, K.; Fujita, Y.; Fukudome, K.; Yamaoka, K. *Polym. J.* **1994**, *26*, 291–302.
(35) Yakobson, B. I.; Couchman, L. S. *J. Nanoparticle Res.* **2006**, *8*, 105–110.
(36) Sano, M.; Kamino, A.; Okamura, J.; Shinkai, S. *Science* **2001**, *293*, 1299–1301.
(37) Buehler, M. J. *J. Mater. Res.* **2006**, *21*, 2855–2869.
(38) Boyd, R.; Sanwal, S.; Shary-Tehrany, S.; McNally, D. *J. Phys. Chem.* **1971**, *75*, 1264–1271.
(39) Mansfield, M. L. Unpublished results.
(40) Tersoff, J. *Phys. Rev. Lett.* **1986**, *56*, 532–635.
(41) Tersoff, J. *Phys. Rev. B* **1988**, *37*, 6991–7000.
(42) Tersoff, J. *Phys. Rev. Lett.* **1988**, *61*, 2879–2882.
(43) Mansfield, M. L. *Macromolecules* **1986**, *19*, 854–859.
(44) We do not ascribe any fundamental significance to the forms of eqs 14, 15, or 22–25, which are just summaries of our numerical data to a given uncertainty. By giving the coefficients and exponents in these equations to 4 significant digits, we are not implying that our integrations have this accuracy, but instead, the inclusion of these digits insures that the reader can reproduce our numerical estimates to within the stated uncertainty.
(45) The volume swept out by a sphere of diameter d translating along a Brownian trajectory obeys a known formula. See: Spitzer, F. *Z. Wahr* **1964**, *3*, 110−121, ref 19, and Jansons, K. M.; Phillips, C. G. *J. Colloid Interface Sci.* **1990**, *137*, 75−91. This implies that in the limit of small ϵ, $V/V_{\mathrm{worm}} \cong 8\epsilon/3\delta$, which becomes arbitrarily small as either ϵ decreases or δ increases. However, because we do not consider ϵ below 0.025, we have not been able to confirm this limit in this study.
(46) Miles, J. W. *J. Appl. Phys.* **1967**, *38*, 192–196.
(47) Mansfield, M. L.; Douglas, J. F. *Macromolecules* **2008,** *41*, 5422–5432.
(48) Goren, S. L.; O'Neill, M. E. *J. Fluid Mech.* **1980**, *101*, 97–110.
(49) Hays, J. B.; Magar, M. E.; Zimm, B. H. *Biopolymers* **1969**, *8*, 531–538.
(50) Borochov, N.; Eisenberg, H.; Kam, Z. *Biopolymers* **1981**, *20*, 231–235.
(51) Sobel, E. S.; Harpst, J. A. *Biopolymers* **1991**, *31*, 1559–1564.
(52) Porschke, D. *Biophys. Chem.* **1991**, *40*, 169–179.
(53) Lu, Y.; Weers, B.; Stellwagen, N. C. *Biopolymers* **2002**, *61*, 261–275.
(54) Eckelt, J.; Knopf, A.; Wolf, B. A. *Macromolecules* **2008**, *41*, 912–918.
(55) Aharoni, S. M. *Macromolecules* **1987**, *20*, 2010–2017.
(56) Bauer, B. J.; Becker, M. L.; Bajpai, V.; Fagan, J. A.; Hobbie, E. K.; Migler, K.; Guttman, C. M.; Blair, W. R. *J. Phys. Chem. C* **2007**, *111*, 17914–17918.

MA702837V